Subanesthetic ketamine exerts antidepressant-like effects in adult rats exposed to juvenile stress

Katsuhiro Aikawa[a] katsuhiro.aikawa@med.hokudai.ac.jp

Takayuki Yoshida[b, c] takyoshi@hiroshima-u.ac.jp

Yu Ohmura[b] yohmura@med.hokudai.ac.jp

Kerise Lyttle[b] keriselyttle305@gmail.com

Mitsuhiro Yoshioka[b] flute@med.hokudai.ac.jp

Yuji Morimoto[a] morim2@med.hokudai.ac.jp

Affiliations

[a]Department of Anesthesiology and Critical Care Medicine, Faculty of Medicine and Graduate School of Medicine, Hokkaido University, Kita-15, Nishi-7, Kita-ku, Sapporo 060-8638, Japan

Phone: +81-11-706-7861

[b]Department of Neuropharmacology, Faculty of Medicine, Hokkaido University, Kita-15, Nishi-7, Kita-ku, Sapporo 060-8638, Japan

Phone: +81-11-706-5059

[c]Department of Neurophysiology, Graduate School of Biomedical and Health Sciences, Hiroshima University, Kasumi 1-2-3, Minami-ku, Hiroshima 734-8551, Japan

Phone: +81-82-257-5127

Declarations of interest: none

Corresponding author: Takayuki Yoshida, Ph.D.

Department of Neurophysiology, Graduate School of Biomedical and Health Sciences, Hiroshima University

Kasumi 1-2-3, Minami-ku, Hiroshima 734-8551, Japan

Phone: +81-82-257-5127

E-mail: takyoshi@hiroshima-u.ac.jp

Abstract

Juvenile stress, like that caused by childhood maltreatment, is a significant risk factor for psychiatric disorders such as depression later in life. Recently, the antidepressant effect of ketamine, a noncompetitive *N*-methyl-*d*-aspartate receptor antagonist, has been widely investigated. However, little is known regarding its efficacy against depressive-like alterations caused by juvenile stress, which is clinically relevant in human depression. In the present study, we evaluated the antidepressant-like effect of ketamine in adult rats that had been subjected to juvenile stress. Depressive-like behavior was assessed using the forced swim test (FST), and electrophysiological and morphological alterations in the layer V pyramidal cells of the prelimbic cortex were examined using whole-cell patch-clamp recordings and subsequent recording-cell specific fluorescence imaging. We demonstrated that ketamine (10 mg/kg) attenuated the increased immobility time caused by juvenile stress in the FST, restored the diminished excitatory postsynaptic currents, and caused atrophic changes in the apical dendritic spines. Ketamine's effects reversing impaired excitatory/inhibitory ratio of postsynaptic currents were also revealed. These results indicated that ketamine could be effective in reversing the depression-like alterations caused by juvenile stress.

Keywords

antidepressant effect, E/I ratio, EPSC, glutamatergic neurotransmission, medial prefrontal cortex, prelimbic,

List of abbreviations

3wFS: 3-week footshock

5-HT: Serotonin

ACSF: Artificial cerebrospinal fluid

AMPA: α-amino-3-hydroxy-5-methyl-4-isoxazolepropionic acid

ANOVA: Analysis of variance

BLA: Basolateral amygdala

EAAT: Excitatory amino acid transporter

EPSCs: Excitatory postsynaptic currents

E/I: excitatory/inhibitory

FST: Forced swim test

HCN: Hyperpolarization-activated cyclic nucleotide-gated

IEI: Inter-event interval

IL: Infralimbic area

IPSCs: Inhibitory postsynaptic currents

Ket: Ketamine

mEPSCs: Miniature excitatory postsynaptic currents

mIPSCs: Miniature inhibitory postsynaptic currents

1 mPFC: medial prefrontal cortex

2 NMDA: *N*-methyl-*d*-aspartate

3 PL: prelimbic area

4 sEPSCs: Spontaneous excitatory postsynaptic currents

5 sIPSCs: Spontaneous inhibitory postsynaptic currents

6 SPT: Sucrose preference test

7 TTX: Tetrodotoxin

8 VEH: Vehicle

1. Introduction

Depression is a mental health disorder characterized by persistent depressive mood and loss of interest. Over 300 million patients worldwide suffer from depression, making it a leading cause of social disability. It is associated with 800 thousand suicides every year and a significant social and economic burden (Kessler et al., 2003; WHO, 2018). Intense juvenile stress, such as child abuse, is a substantial cause of depression later in life (Anda et al., 2010; Heim and Nemeroff, 2001; Lupien et al., 2009). Studies suggest that juvenile stress induces epigenetic alterations in the immature brain, which lead to an increased risk for psychiatric disorders (Menke and Binder, 2014). Juvenile stress also induces atrophic changes in the pyramidal cells of the medial prefrontal cortex (mPFC) (strongly associated with mood control and cognitive function in humans (Drevets et al., 1997; Sullivan and Gratton, 2002)) and increases depressive-like behavior in adult rodents (Lyttle et al., 2015; Yamamuro et al., 2018). These findings indicate that glutamatergic neuronal deficits in the mPFC, caused by juvenile stress, may be strongly associated with depression in adulthood. Furthermore, Tunnard et al. (Tunnard et al., 2014) demonstrated an association between child abuse and depression with treatment resistance and suicidal ideation. This indicates a complex mechanism for depression induced by juvenile stress. In recent years, the non-competitive *N*-methyl-*d*-aspartate

(NMDA) receptor antagonist, ketamine, has gathered marked attention as a rapid-acting antidepressant (Berman et al., 2000; Duman, 2018; Zarate et al., 2006) when administered at subanesthetic doses (5-30 mg/kg) (Li et al., 2010; Wu et al., 2020). While ketamine's effectiveness for treatment-refractory depression has been reported (Wilkinson et al., 2018), its efficacy against depression originating from juvenile stress is poorly understood. Such information is clinically relevant for human depression.

In the present study, we examined whether ketamine exerts an antidepressant-like effect in adult rats that had experienced juvenile stress, using a 3-week footshock (3wFS) model (Hiraide et al., 2012; Kimura et al., 2011; Lyttle et al., 2015; Matsuzaki et al., 2011). The forced swim test (FST) and sucrose preference test (SPT) were used to evaluate the antidepressant-like effect of ketamine. The whole-cell patch-clamp recordings and the subsequent morphological examination of the mPFC layer V pyramidal cells, which preferentially receive synaptic inputs from the ventral hippocampus (Carreno et al., 2016), were used to study the underlying behavioral mechanisms. The pyramidal neurons at layer V of the mPFC mainly integrate information from other brain areas and are the main output source from the mPFC. Moreover, the distal dendrites of the layer V pyramidal cells are especially sensitive to chronic stress (Liu and Aghajanian, 2008). To verify that an appropriate balance of excitatory and inhibitory inputs is essential for the normal brain

function, we investigated the alterations of excitatory postsynaptic currents (EPSCs) and inhibitory postsynaptic currents (IPSCs) caused by juvenile stress and ketamine (Gerhard et al., 2019; Workman et al., 2018).

2. Results

Rats were randomly assigned to one of the following four groups: non-footshock + vehicle administration (noFS-VEH), noFS + ketamine treatment (noFS-Ket), 3wFS + VEH (3wFS-VEH), and 3wFS + Ket (3wFS-Ket). The time course of exposing the rats to juvenile stress and administering ketamine or saline is shown in Fig. 1.

2.1. Ketamine reverses depressive-like behavior caused by juvenile stress in the FST

We employed the FST to evaluate the antidepressant-like properties of ketamine by comparing immobility, which represents non-escape-related behaviors, among the four groups (Fig. 2). A two-way analysis of variance (ANOVA) identified a significant 3wFS × ketamine interaction ($F_{(1, 27)} = 17.185$, $P < 0.001$). Significant differences between the noFS-VEH and 3wFS-VEH ($P = 0.007$), and 3wFS-VEH and 3wFS-Ket ($P = 0.004$), and noFS-Ket and 3wFS-Ket groups ($P = 0.007$) were revealed, indicating that ketamine attenuates the increased immobility by 3wFS. Interestingly, ketamine paradoxically increased the immobility counts in the noFS groups ($P = 0.011$; Fig. 2).

Next, we assessed the dose-dependency of ketamine for immobility in the 3wFS rats (Fig. S1). Although the statistical analysis was not performed due to the repetitive use of

the data, 1 mg/kg ketamine did not reduce the immobility counts. This indicates that an insufficient dose of ketamine does not exert antidepressant-like effects, similar to previous findings in chronic stress models (Zanos et al., 2016).

2.2 3wFS-rats did not show anhedonia-like behavior in the SPT.

To test the anhedonia-like alteration by 3wFS, we performed the SPT (Fig. S2). No significant difference was detected between noFS and 3wFS groups ($t_{(12)}$ = 0.893, P = 0.39: Student's t-test). This result indicates that 3wFS does not induce anhedonia-like alteration in adulthood.

2.3. Ketamine increases input resistance of layer V pyramidal cells in the prelimbic cortex

To examine the alterations of neuronal excitability, we tested the effects of 3wFS and ketamine using current-clamp recording (Fig. 3). We did not find any interaction of 3wFS × ketamine × current (three-way ANOVA, $F_{(1.729,\ 53.597)}$ = 0.293, P = 0.715), but we observed that ketamine increased the firing frequency ($F_{(1,\ 31)}$ = 32.388, P < 0.001; Fig. 3C). Regarding input resistance, a two-way ANOVA showed no 3wFS × ketamine interaction ($F_{(1,\ 31)}$ = 0.213, P = 0.648), but identified a main effect of ketamine enhancing

input resistance ($F_{(1, 31)}$ = 4.751, P = 0.037; Fig. 3E), while there were no significant differences in the resting membrane potential (Fig. 3F). These results indicate that ketamine increases the firing frequency by enhancing the input resistance of the layer V pyramidal cells in the prelimbic area (PL). Conversely, in the infralimbic area (IL), we did not find any significant differences in the firing pattern, membrane resistance, or resting membrane potential (Fig. S2A−D).

2.4. Ketamine rescues excitatory postsynaptic currents attenuated by 3wFS

Using voltage-clamp recordings, we monitored the spontaneous EPSCs (sEPSCs) to analyze the alteration of the excitatory synaptic inputs in the PL pyramidal neurons of each group (Fig. 4). Representative traces are shown in Fig. 4A. Regarding the sEPSC amplitude, we found no significant 3wFS × ketamine interaction ($F_{(1, 60)}$ = 0.185, P = 0.669) and effect of 3wFS ($F_{(1, 60)}$ = 2.077, P = 0.155) or ketamine ($F_{(1, 60)}$ = 2.3, P = 0.135; Fig. 4B). In the inter-event intervals (IEIs) of sEPSC, a significant 3wFS × ketamine interaction ($F_{(1, 60)}$ = 10.943, P = 0.002) was identified. There were significant differences in the IEIs between the noFS-VEH and 3wFS-VEH (P < 0.001), and the 3wFS-VEH and 3wFS-Ket groups (P = 0.002, Fig. 4C). The latter indicated that ketamine reversed the decrease in sEPSC frequency.

Then, we investigated the miniature EPSCs (mEPSCs) by utilizing tetrodotoxin (TTX), to further obtain insights in the alteration of the presynaptic glutamate release and/or properties of postsynaptic receptors induced by 3wFS and ketamine.

Representative traces of mEPSCs are shown in Fig. 4D. Regarding the amplitude, we observed a significant 3wFS × ketamine interaction ($F_{(1, 53)}$ = 10.958, P = 0.002). We further found a significant difference between the noFS-VEH and 3wFS-VEH (P = 0.036), and 3wFS-VEH and 3wFS-Ket groups (P = 0.008, Fig. 4E). In the mEPSC IEIs, a significant 3wFS × ketamine interaction was detected ($F_{(1, 53)}$ = 12.956, P < 0.001). There were significant differences between the noFS-VEH and noFS-Ket (P = 0.042) and the 3wFS-VEH and 3wFS-Ket (P = 0.042), and the noFS-Ket and 3wFS-Ket groups (P = 0.001). Furthermore, there was a tendency of significant effect of 3wFS in the VEH group (P = 0.093; Fig. 4F). These results suggested that 3wFS attenuates excitatory inputs, and ketamine restores them.

2.5. Ketamine increased the amplitude of sIPSCs, and 3wFS increased the frequency of mIPSCs

Representative traces are shown in Fig. 5A. Regarding the spontaneous IPSCs (sIPSCs) amplitude, we did not observe a significant 3wFS × ketamine interaction ($F_{(1,}$

$_{40)}$ = 0.152, P = 0.699) or a main effect of 3wFS ($F_{(1, 40)}$ = 0.027, P = 0.87), but observed a significant main effect of ketamine was evident (P = 0.006; Fig. 5B). Regarding the sIPSC IEIs, there were no significant interactions ($F_{(1, 40)}$ = 2.236, P = 0.143) or a main effect of 3wFS ($F_{(1, 40)}$ = 2.121, P = 0.153) and ketamine ($F_{(1, 40)}$ = 0.079, P = 0.78; Fig. 5C) were observed.

Representative mIPSCs traces are shown in Fig. 5D. Regarding the amplitude, there were no significant interactions ($F_{(1, 35)}$ = 0.324, P = 0.573) or main effects of 3wFS ($F_{(1, 35)}$ = 1.411, P = 0.243) and ketamine ($F_{(1, 35)}$ = 1.267, P = 0.268, Fig. 5E). No significant interaction was found in the mIPSC IEIs ($F_{(1, 35)}$ = 0.206, P = 0.653) or main effects of ketamine ($F_{(1, 35)}$ = 0.608, P = 0.441), but there was a significant main effect of 3wFS ($F_{(1, 35)}$ = 5.26, P = 0.028) was identified (Fig. 5F).

2.6. Ketamine reversed impaired excitatory/inhibitory (E/I) ratio by 3wFS

As balanced excitatory and inhibitory inputs are essential for the healthy brain function (Workman et al., 2018), the E/I ratio of charge and IEI was calculated with the data obtained from the same cells (Fig. 6). Regarding the E/I ratio of the charge, there was a lack of interaction ($F_{(1, 32)}$ = 0.350, P = 0.558) or main effects of 3wFS ($F_{(1, 32)}$ = 0.019, P = 0.890) and ketamine ($F_{(1, 32)}$ = 0.351, P = 0.557; Fig. 6A). In the E/I ratio of

the IEI, significant 3wFS × interaction was identified ($F_{(1, 32)}$ = 17.14, P = 0.011). Significant differences between the noFS-VEH and 3wFS-VEH groups (P = 0.041), the 3wFS-VEH and 3wFS-Ket groups (P = 0.004), and a tendency of significance between the noFS-VEH and noFS-Ket groups (P = 0.094) were found (Fig. 6B). These results indicated that ketamine restored decreased excitatory neurotransmission, and that ketamine exerted antidepressant-like effect by reversing impaired E/I ratio in the mPFC.

2.7. Ketamine restored atrophic changes in apical dendritic spines, while there was no significant change in the basal dendritic spines

Stress and depression induce neuronal atrophy and a decreased number of synapses in the mPFC that are associated with depressive-like behaviors in rodent models (Duman, 2018). We analyzed the alterations of spine density and the proportion of mature spines, which are associated with a stronger glutamatergic synaptic transmission (Moench and Wellman, 2015). The data obtained from the dendritic areas are shown in Fig. 7A. The average measured lengths of the apical dendrites [mean ± standard error of the mean (SEM)] were as follows: noFS-VEH, 112 ± 6.6 μm; noFS-Ket, 111 ± 4.5 μm; 3wFS-VEH, 115 ± 4.6 μm; and 3wFS-Ket, 118 ± 7.6 μm. A significant 3wFS × ketamine interaction was identified in the apical dendritic spine density (two-way ANOVA, $F_{(1, 39)}$ = 5.418, P

= 0.025). Further, 3wFS decreased the spine density in the VEH group ($P < 0.001$; Fig. 7B), a trend that was reversed by ketamine in the 3wFS groups ($P = 0.097$). Regarding the proportion of the mature spines, a two-way ANOVA identified a lack of interaction between 3wFS and ketamine ($F_{(1, 39)} = 1.902$, $P = 0.176$), and revealed a main effect of ketamine ($F_{(1, 39)} = 10.044$, $P = 0.003$; Fig. 7C), indicating that ketamine rescued the atrophic changes of the spine, congruent with the results of previous studies (Li et al., 2010; Liu et al., 2015). In contrast, there were no significant differences in the basal dendritic spine density and the proportion of the mature spines (Fig. 7 E–G). The average measured lengths of basal dendrites (mean ± SEM) were as follows: noFS-VEH, 119 ± 4.8 μm; noFS-Ket, 126 ± 6.8 μm; 3wFS-VEH 109 ± 5.2 μm; and 3wFS-Ket, 103 ± 6.1 μm.

3. Discussion

The main findings of the present study were: (1) subanesthetic doses of ketamine in adult rats reversed the behavioral, excitatory and inhibitory neurotransmissional, and morphological alterations diminished by juvenile stress; and (2) ketamine paradoxically exhibited prodepressant-like effects in the noFS rats.

Although the mechanisms behind ketamine's antidepressant effect have not been well examined, previous electrophysiological studies have strongly indicated that restoring EPSCs plays a critical role (Duman and Aghajanian, 2012; Zanos et al., 2018). Our analyses on the FST, EPSCs, the balance of synaptic excitation and inhibition, and apical dendritic spine imaging indicated that 3wFS induced depressive-like alteration during adulthood and that ketamine attenuated this effect, consistent with previous studies using chronic stress models (Li et al., 2010; Li et al., 2011). To our knowledge, this is the first study that analyzed the ketamine's antidepressant effect on juvenile stress-induced alteration in rodents, which is a major cause of depression in humans (Anda et al., 2010). However, further studies are required to extrapolate these results to humans.

We demonstrated that 3wFS increased the immobility counts in adult rats and that ketamine reversed this increase (Fig. 2). Although we did not measure ketamine's effect on the locomotor activity, previous studies reported that ketamine 10 mg/kg transiently

increased locomotion in the very early period (~ 1 h) and promptly reversed it to the placebo levels (Hetzler and Wautlet, 1985; Podkowa et al., 2016). As we injected ketamine 16 h before the FST, the significant differences in immobility in the FST between the noFS-VEH, 3wFS-VEH, and 3wFS-Ket groups could not be attributed to the alteration in the locomotor activity. Furthermore, ketamine 1 mg/kg did not reverse immobility in our study, similar to other reports (Fig. S1) (Li et al., 2010; Zanos et al., 2016).

Interestingly, we demonstrated that ketamine increased the firing frequency and input resistance in the PL, but not in the IL (Fig. 3 and Fig. S2). This suggested that the effects of ketamine on the PL neurons might be different from those on the IL neurons. There are pyramidal neurons in the IL and PL, but the effects of the drug could be different between them. For example, our previous report (Lyttle et al. 2015) showed that repeated fluvoxamine treatment recovered stress-induced dendritic atrophy in the IL but not in the PL, though it examined the layer II/III. Moreover, several studies indicated that the IL plays a pivotal role in the antidepressant-like effects (Hamani et al., 2010a; Hamani et al., 2010b; Hamani and Temel, 2012; Lyttle et al., 2015). Taken together with previous and present findings, we speculated that the recovery of PL or IL is sufficient for antidepressant-like effects, but the recovered region depends on the type of the used drug.

However, further studies are required to elucidate how and why drugs seemingly have differing effects on the same type of neurons in different areas. Further, ketamine might affect other brain regions than the IL or PL and indirectly induce plastic changes of pyramidal neurons, depending on the source of inputs.

Increased firing frequency is not likely a result of ketamine's effect on input resistance, because those in the noFS-Ket and 3wFS-VEH groups were almost the same (Fig. 3E). A recent study reported that a low dose of ketamine increased the spontaneous firing of mPFC pyramidal neurons by attenuating the small conductance calcium-activated potassium channel-mediated action potential hyperpolarization current and rapidly enhanced mPFC neuronal excitability within the therapeutically relevant time window (Bambico et al., 2020). The increment of input resistance was due to the decrease of ion permeability on the membrane. A previous study reported that input resistance was increased by blockade of the hyperpolarization-activated cyclic nucleotide-gated (HCN) channels in the CA1 pyramidal neuron (Surges et al., 2004), and it has also been reported that ketamine inhibits HCN1 and increases the efficacy of cortical inputs (Chen et al., 2009; Ku and Han, 2017; Wang et al., 2007). Further investigation is required to test the aforementioned possibilities.

The synaptic current analysis demonstrated that 3wFS diminished the sEPSC

frequency in adulthood, which could cause increased immobility and reflect depressive-like alteration by juvenile stress (Menke and Binder, 2014; Yamamuro et al., 2018). As ketamine's antidepressant effect works by enhancing EPSC in the mPFC (Li et al., 2010; Li et al., 2011; Liu et al., 2015), it is reasonable to assume that ketamine recovers the excitatory inputs altered by juvenile stress. By investigating the mEPSCs, we further demonstrated the significance in the amplitude, and the tendency of significance in the IEI. These parameters generally indicate the change in the functions of postsynaptic receptors and the probability of action potential-independent presynaptic glutamate release, respectively (Arborelius and Eklund, 2007; Ishikawa et al., 2002; Oertner et al., 2002). Although the effects of ketamine on the presynaptic terminals remain unclear, a previous report has shown that subanesthetic ketamine restores the function of the excitatory amino acid transporter 3 (EAAT3) and alleviates the depressive-like behavior in rats (Zhu et al., 2017). However, as EAAT3 is located on the pre- and postsynaptic regions of the neurons found in the hippocampus and the cortex, further examination is required to clarify the ketamine's presynaptic modulations in the mPFC. Consistent with previous reports on the effects of ketamine on postsynaptic sites (Duman et al., 2016; Duman, 2018; Liu and Aghajanian, 2008), we also demonstrated that the administration of ketamine in 3wFS rats restored the EPSC amplitude reflecting the number of α-amino-

3-hydroxy-5-methyl-4-isoxazolepropionic acid (AMPA) receptors, spine density, and the percentage of the mushroom-shaped maturated spine, resulting in postsynaptic potentiation via the AMPA receptors (Gould et al., 2019). It is also possible that the increased amplitude of the EPSC was due to a change in the presynaptic vesicle content (Yu et al., 2018). Recent studies suggested that ketamine blocks the NMDA receptors on the neurotransmitter gamma-aminobutyric acid (GABA)-ergic interneurons and causes disinhibition, subsequently leading to the synaptogenesis of AMPA receptors (Duman and Aghajanian, 2012). However, there is the possibility that ketamine activates the prefrontal serotonergic system through an AMPA receptor-independent mechanism (Ago et al., 2019).

Cortical circuits are composed of excitatory glutamatergic pyramidal neurons and inhibitory GABAergic interneurons, which together create a delicate balance of excitation and inhibition (Workman et al., 2018; Xue et al., 2014). Moreover, we also measured the IPSCs and calculated the E/I ratio. Our study demonstrated that ketamine increased the sIPSCs amplitude (Fig. 5B), and that the 3wFS reduced the mIPSCs IEI (Fig. 5F). Previous studies proposed a putative mechanism that involves preferential ketamine-mediated inhibition of NMDA receptors localized in the interneurons, followed by disinhibition of the glutamatergic pyramidal neurons and an increased release of

glutamate (Miller et al., 2016). In fact, the ketamine's effect on IPSCs in the cortical pyramidal neurons remains unclear. The mPFC layer V pyramidal neurons are the main output source to other brain regions, and the net activity of the mPFC is controlled by integrating the excitatory and inhibitory inputs into those neurons (Ferguson and Gao, 2018).

The E/I balance has been shown to change during the early development of the pyramidal neurons (Kroon et al., 2019), and these alterations have been found in rodent models of psychiatric disorders (Chen et al., 2020; Gatto and Broadie, 2010). The current study revealed that 3wFS increased the E/I ratio in the IEI of spontaneous postsynaptic currents, and ketamine reversed this change, indicating that ketamine reversed diminished excitability in the mPFC (Fig. 6). The input from the ventral hippocampus is a likely candidate due to the distribution of terminals, which are concentrated in the mPFC (Carreno et al., 2016; Liu and Carter, 2018). Taken together, our results indicated that ketamine increased the excitatory inputs, restored the E/I balance in the PL, and might contribute to the antidepressant mechanisms underlying the ventral hippocampus-PL E/I balance.

As aforementioned, our results showed that ketamine reversed the synaptic loss in the apical dendrites caused by stress (Fig. 7). However, consistent with previous reports, no

significant changes were observed in the basal dendrites (Cook and Wellman, 2004; Liu and Aghajanian, 2008; Radley et al., 2004). Additionally, a previous report (Liu and Aghajanian, 2008) showed that the apical dendritic regions predominantly generate serotonin (5-HT)-induced EPSCs in the layer V mPFC pyramidal neurons and a significant decrease of EPSCs in stressed rats. Considering that ketamine increases 5-HT release in the mPFC (Ago et al., 2019), our observed selective synaptogenesis in the apical dendrites might indicate the ketamine's direct (with the subsequent promotion of protein synthesis via the activation of the mechanistic target of rapamycin complex 1) and indirect antagonistic effect on the postsynaptic NMDA receptors (Duman, 2018).

As ketamine exerts its peak antidepressant effect within 24 h (Krystal et al., 2013; Pešić et al., 2016; Zarate et al., 2013), the most preclinical studies performed their morphological investigations at 24 h after ketamine's administration, demonstrating a significant recovery in both spine density and the proportion of the matured spines (Li et al., 2010; Li et al., 2011; Zanos et al., 2016). However, the time course between spinogenesis and behavioral changes remains unclear, while previous studies reported that the immobility reversal by ketamine precedes the spine formation by at least 9 h (Moda-Sava et al., 2019). We conducted the examinations at 16 h after ketamine administration, as it would provide some insights into the halfway point of the

antidepressant-like changes. Our results showed that the proportion of the matured spines increased, while the spine density remained unchanged. Previous findings and our results showed that recovery of glutamatergic transmission in the early period was accomplished by the maturation of the existing spines, followed by spine regeneration. A previous study (Li et al., 2010) reported increased levels of synaptic signaling proteins 2 h after ketamine administration. This signifies that synaptogenesis induced by ketamine could occur very rapidly, which is congruent with the clinical appearance (Berman et al., 2000). Thus, our results may suggest a synaptogenesis time course in the apical dendritic spines of the pyramidal cells in the PL layer V. The restoration tendency of spine density between 3wFS-VEH and 3wFS-Ket groups could support this hypothesis.

Our finding that ketamine increased immobility in noFS rats is in conflict with those of previous studies (Autry et al., 2011; Carreno et al., 2016; Li et al., 2010; Maeng et al., 2008) showing ketamine's antidepressant effect using naïve animals. However, our EPSC/IPSC results (increased mEPSC IEI and increased sIPSC amplitude than the corresponding in the noFS-VEH group) indicated impaired excitability in the mPFC, which is consistent with increased immobility in the FST (Li et al., 2011). Therefore, at least in our experimental condition, we are reasonably sure that ketamine worked as a prodepressant agent. This was an unexpected result and warrants further investigation.

However, it was beyond the scope of this study because our main goal was to examine the effects of ketamine on 3wFS model rats, not on control rats. At this point, it remains an open question.

However, our study had some limitations. First, although there are some reports indicating that the human mPFC is involved in depression (Scheinost et al., 2018; Treadway et al., 2015), the idea that the rat mPFC can be considered homologous to human mPFC is still controversial (Uylings et al., 2003). Second, although we have reported that 3wFS induced various depressive-like alterations in the adult rats, this model only reflects a part of depression-like symptoms (Lyttle et al., 2015). For example, in our study, 3wFS did not change the anhedonia-like behavior in the SPT. To assess the ketamine's antidepressant-like effect for juvenile stress, different models like maternal separation should be investigated in future studies. Third, the number of samples used in electrophysiological experiments is relatively low. Although the most *P*-values in insignificant comparison were greater than 0.1, we could miss the significant difference due to the small sample size.

In conclusion, we demonstrated that ketamine reversed depressive-like alterations caused by juvenile stress in adult rats. Using electrophysiological and morphological methods to examine the PL layer V pyramidal cells, we showed that the excitatory inputs

derived from the apical dendrites might play a critical role in the antidepressant effect of ketamine. Furthermore, pre- and post-synaptic factors contributed to the alteration of the EPSCs. The recovery of the diminished glutamatergic transmission in the early period could be due to synaptic maturation. We observed that ketamine had a pro-depressant effect in noFS rats, which is of significant interest to basic research on depression. Finally, we suggested the contribution of IPSCs in the ketamine's antidepressant effect. We believe that these findings could contribute to elucidate the pathophysiology of depression and its therapeutic process.

4. Experimental Procedure

4.1 Animals

We used male offspring of timed-pregnant Wistar/ST rats purchased from Japan SLC (Shizuoka, Japan). The rats were weaned on postnatal day (PND) 21 and group-housed at 21 ± 2°C and relative humidity of 40–50% with a 12-h light-dark cycle (lights on at 19:00). Food and water were provided ad libitum, and all experiments were conducted during the dark period. All procedures were conducted in accordance with the guidelines for the Care and Use of Laboratory Animals of the Animal Research Committee of the Hokkaido University. In total, 74 animals were included.

4.2 Juvenile stress exposure

A juvenile stress paradigm was used, based on our previous reports (Lyttle et al., 2015; Matsuzaki et al., 2011). On PND 21, rat pups were weaned and received an electric foot shock once a day until PND 25. The time course of the experiments and the protocol of juvenile stress induction are shown in Fig. 1A. Rat pups were randomly assigned to an inescapable electric foot shock (3wFS) or a noFS group. Each rat was acclimated in the foot shock box for 5 min and subsequently subjected to five series of electrical foot shocks (intensity, 0.5 mA; duration, 2 s; and inter-shock interval, 30 s). The rat pups remained in

the foot shock box for another 5 min after the last foot shock and then returned to their home cage. The rats assigned to the noFS group were acclimated in the foot shock box for the same time as the FS rats (12.5 min) without receiving an electric shock. After being subjected to juvenile stress, the rats were group-housed in the same setting, as aforementioned, until PND 70, and they were subjected to experiments between the PND 70 and PND 90.

4.3 Sucrose preference test

To test anhedonia-related behavior induced by 3wFS, the SPT was performed. Our procedure here was based on the Willner's method (Willner et al., 1987). The rats were singly housed for a period of 7 days prior to the start of sucrose preference testing. The rats were not deprived of food or water before or during the test. Sucrose preference testing started with a habituation interval of 24 h. During the habituation period, the rats received two bottles of a 1% sucrose solution. Following the habituation period, three baseline measures of sucrose preference were taken. A third day of baseline period was selected based on preliminary experiments. For assessment of baseline sucrose preference, the rats were provided 200 ml of tap water and 200 ml of a 1% sucrose solution. The bottle positions were counterbalanced each successive day to prevent place preference.

The consumption of water and sucrose solution was measured by weighing the bottles. Sucrose preference was calculated as the percentage of the division between the sucrose solution and the total consumptions.

4. 4 Drug administration

Based on previous reports (Li et al., 2010; Zanos et al., 2018), the animals in both groups received 10 mg/kg racemic ketamine (Ket; Daiichi Sankyo, Tokyo, Japan) or 0.9% saline (vehicle, VEH) intraperitoneally, approximately 16 h before the experiments (Fig. 1B). Ketamine was dissolved in a total volume of 2 mL of a saline solution immediately prior to the injection.

4.5 Forced swim test

The FST was conducted on PND 70, according to our previous report (Lyttle et al., 2015). A cylindrical acrylic container (20-mm inner diameter × 600-mm height) filled up to 450 mm with water (25 ± 1°C) was used. The rats were recorded for 15 min, and the behavioral parameters were measured by hand count at the end of each 5-s interval (Jutkiewicz et al., 2006; Lyttle et al., 2015). Immobility was defined as no additional activity other than required to keep the rats' heads above water. The counts of immobility

were compared among the four groups. The counting procedure was performed in a blinded manner. The rats exposed to the FST were not used for other experiments, as the test itself can be a significant stressor and affect the results of other experiments (Sarkar and Kabbaj, 2016). Further, to investigate the dose-dependent effects of ketamine, a group of 3wFS-subjected rats was administered with 1 mg/kg ketamine.

4.6 Brain slice preparation

Brain slice preparation was performed according to our previous report (Tsutsui-Kimura et al., 2014). Briefly, after decapitation under CO_2 anesthesia, the rats' brains were rapidly removed and placed in an ice-cold low-Na^+ solution containing (in mM) 120 choline-Cl, 3 KCl, 1.25 NaH_2PO_4, 28 $NaHCO_3$, 8 $MgCl_2 \cdot 6\ H_2O$, and 22 d-glucose (pH 7.4), aerated with 95% O_2 and 5% CO_2. Next, 300-μm acute transverse slices containing the mPFC were cut using a VT1200S slicer (Leica, Heidelberg, Germany). For tissue recovery, slices were incubated for 30 min at 35°C in a 1:1 mixture of low-Na^+ solution and normal artificial cerebrospinal fluid (ACSF) containing (in mM) 125 NaCl, 2.5 KCl, 2 $CaCl_2$, 1 $MgSO_4$, 1.25 NaH_2PO_4, 26 $NaHCO_3$, and 20 d-glucose (pH 7.4), followed by another 30 min at 25°C in ACSF aerated with 95% O_2 and 5% CO_2.

4.7 Electrophysiological recordings

Whole-cell patch-clamp recordings were obtained from the layer V pyramidal cells in the PL, based on our previous report (Shikanai et al., 2012). We utilized an upright microscope (BX51WI, Olympus, Tokyo, Japan) equipped with an infrared charge-coupled device camera system (IR filter-removed DP72; Olympus) in ACSF at 32°C. Recording pipets with 3−5-MΩ resistance were used. For stimulation and data acquisition, an Axopatch 200B amplifier and the Clampex 10.6 software (Molecular Devices, Sunnyvale, CA, USA) were utilized. Signals were digitized at 20 kHz and filtered with a low-pass Bessel filter at 3 kHz. Clampfit 10.4 (Molecular Devices) was used for data analysis.

A standard intracellular solution containing (in mM) 6 KCl, 130 K_D-gluconate, 10 NaCl, 0.5 EGTA, 2 $MgCl_2$, 0.16 $CaCl_2$, 10 HEPES, 4 (2Na)-ATP, and 0.4 (2Na)-GTP (pH 7.3) was used in current-clamp recordings. After holding the pyramidal cells at -60 mV, the recording was started in the current-clamp mode. A stepwise current injection (intensity, -0.2−0.5 nA with 0.05-nA increments; duration, 500 ms) was administered, and the changes in membrane potentials were recorded. The liquid junction potential was approximately 9 mV between the pipette solution and ACSF and was subtracted from the recorded data.

We designed the procedure to obtain the data of EPSCs and IPSCs from the same cell at comparable times (Kroon et al., 2019) using the cesium-based internal solution, containing (in mM) 7.5 CsCl, 127.5 Cs-methanesulfonate, 0.6 EGTA, 10 HEPES, 2.5 $MgCl_2$, 4 Na_2-ATP, 0.4 Na_3-GTP, and 10 Na_2 phosphocreatine was used in voltage-clamp recordings, which was adjusted to match the physiological intracellular Cl^- concentration (12.5 mM) in the mature neurons. sEPSCs and sIPSCs were recorded at -70 and 0 mV, respectively. To record mEPSCs and mIPSCs, 0.5 μM TTX (Nacalai Tesque) was applied in the ACSF. The data were obtained at least 10 min after drug application to establish the appropriate effects. To confirm the validity of our experimental design, we verified that the postsynaptic currents clamped at -70 and 0 mV were totally blocked by 3 mM kynurenic acid (Sigma, St. Louis, MI, USA) and 0.1 mM picrotoxin (Nacalai Tesque, Kyoto, Japan), respectively. sIPSC and mIPSC were recorded within 1 min immediately after changing the holding potential from -70 to 0 mV. Pipet capacitance and series resistance compensation, or bridge-balance adjustments, were performed in voltage- or current-clamp mode, respectively, as follows: the series resistance was <10 MΩ; the maximal residual voltage error was <10%; the pipet offset potential between was zeroed before the gigaohm seal was established. Mini Analysis (Synaptosoft Inc, Decatur, GA, USA) was used for data analysis of the amplitude (pA), IEI (ms), and charge (fC) of

postsynaptic currents. Three times the RMS value of baseline was set as the threshold for signal detection for each recording. The other detection parameters were set as follows; Period to search a local maximum (μs): 10,000 for EPSCs and 20,000 for IPSCs, time before a peak for baseline (μs): 5,000 for EPSCs and 10,000 for IPSCs, period to search a decay time (μs): 20,000 for EPSCs and 40,000 for IPSCs, fraction of peak to find a decay time: 0.37, period to average a baseline (μs): 500. The acquired data (30-s) were manually inspected to reject the false events caused by noise and to include events that were not detected automatically.

4.8 Dendritic spine analysis

Morphological analyses of dendritic spines were performed as previously described (Tsutsui-Kimura et al., 2014). Biocytin (0.1%; Nacalai Tesque) was added to the intracellular solution for the following morphological analysis. After whole-cell recordings, slices were transferred to 4% paraformaldehyde (0.1 M phosphate buffer) and fixed overnight at 4°C. Subsequently, slices were processed with streptavidin conjugated to Alexa 488 (1:1000; Jackson Immuno Research, Westgrove, PA, USA) to visualize the recorded pyramidal cells. A 3D image was obtained utilizing an FV1000 confocal laser microscope with FV10-ASW ver3.1 software (Olympus). Apical and basal dendritic

spines were recorded under 60× objective, 2× digital zoom, and Z-stacks at 0.5-μm steps. The criteria for the area from which the images were obtained were as follows: for apical dendrites, (1) just distal from the bifurcation of the main shaft (“tufts”), (2) within 200 μm from the pia, (3) >1-μm diameter tuft in the acquired image, to compare tufts with the similar condition; for basal dendrites, we excluded the spine-sparse area next to the soma. The typical area from which we obtained images is shown in Fig 6A. Spine head diameter and density were measured from the obtained images. For processing and analysis of acquired images, Image J (Schneider et al., 2012) and SPISO (Mukai et al., 2011) were used. Since spine diameter correlates with synaptic strength, we sorted the spines into two types based on their transverse diameters: mature (>0.8 μm) or immature (<0.8 μm).

4.9 Statistical analysis

Statistical analysis was performed using SPSS Statistics version 23 (IBM Corp., Armonk, NY, USA). The most data were analyzed using two-way ANOVA. When the data were not normally distributed, the Aligned Rank Transform (Wobbrock et al., 2011) was employed to detect the interaction effects or main effects. Because we have only two groups for each factor (noFS versus 3wFS, or vehicle versus ketamine), we did not conduct post hoc tests when we found main effects without a significant interaction

between two factors. When a significant interaction was detected, the simple main effects were calculated to assess the difference at each level. As for the Aligned Rank Transformed data, the Wilcoxon signed-rank test with Holm's correction was utilized when a significant interaction was detected. For firing frequency analysis, a three-way ANOVA was utilized by adding a current intensity factor. The Greenhouse−Geisser correction was applied when the results of the Mauchly sphericity test were found to be significant. The statistically significant level was set at $P < 0.05$.

Acknowledgments

We would like to thank Naoya Nishitani (Kanazawa University) and Takesi Izumi (Health Science University of Hokkaido) for their technical advices and assistance in the drafting of the manuscript and Mao Nebuka, Hitomi Sasamori, Wang Ce, Midori Kobie, and Aki Tanimori (Hokkaido University) for helping rear the animals.

Funding

This work was supported by JSPS KAKENHI Grant-in-Aid for Scientific Research(C) [Grant Number JP16K10182 (TY)].

Figure legends

Fig. 1. Experimental time course and juvenile stress protocol

(A) Rat pups were weaned at PND 21 and exposed to foot shock once a day until PND 25. The black electric marks indicate each foot shock. Each rat pup was acclimated in the foot shock box for 5 min and subjected to five electric foot shocks (intensity, 0.5 mA; inter-shock interval, 30 s; shock duration, 2 s). The rat pups were returned to their home cage 5 min after the last foot shock. (B) Between PND 70 and 90, the rats received ketamine or saline injection intraperitoneally approximately 16 h before the subsequent experiments.

FST: forced swim test; PND: postnatal day

Fig. 2. Ketamine rescues increased immobility counts induced by juvenile stress

Effects of juvenile stress (foot shock, 3wFS) and ketamine on the immobility counts in the FST on PND 70. Data are expressed as means ± standard error of the mean. Statistics were calculated by two-way analysis of variance. *, $P < 0.05$; **, $P < 0.01$; simple main effect of 3wFS or ketamine. The number of animals in the groups was as follows; noFS-VEH, 7; noFS-Ket, 10; 3wFS-VEH, 7; and 3wFS-Ket, 7. noFS-VEH: non-footshock + vehicle administration; noFS-Ket: non-footshock + ketamine treatment; 3wFS-VEH: 3-

week footshock + vehicle administration; 3wFS-Ket: 3-week footshock + ketamine treatment; FST: forced swim test; PND: postnatal day

Fig. 3. Ketamine increases firing rates in the prelimbic area layer V pyramidal cells

(A) Schematic of an acute transverse slice containing mPFC. The square corresponds to the area photographed in B. (B) Representative photograph during the whole-cell patch-clamp recording from the PL layer V pyramidal cells. Scale bar, 100 μm. (C and D) Membrane potential changes in the PL layer V pyramidal cells evoked by positive current injection (C) and representative recordings (D). (E and F) Membrane resistance (E) and RMP (F) in the PL layer V pyramidal cells. Data are expressed as means ± standard error of the mean. Statistics were calculated by a three-way or two-way analysis of variance. #, $P < 0.05$; ##, $P < 0.01$; main effect of ketamine. The number of animals and cells in each group for data acquisition was as follows: (animals, cells): noFS-VEH (6, 9), noFS-Ket (4, 12), 3wFS-VEH (5, 7), and 3wFS-Ket (3, 7). IL: infralimbic; PL: prelimbic; noFS-VEH: non-footshock + vehicle administration, noFS-Ket: non-footshock + ketamine treatment, 3wFS-VEH: 3-week footshock + vehicle administration, 3wFS-Ket: 3-week footshock + ketamine treatment; mPFC: medial prefrontal cortex; RMP: resting membrane potential.

Fig. 4. Ketamine reverses the diminished spontaneous and miniature excitatory postsynaptic currents

(A) Representative data of sEPSCs of each group. (B and C) Amplitude (B) and IEI (C) of sEPSCs in PL layer V pyramidal cells. (D) Representative data of mEPSCs of each group. (E and F) Amplitude (E) and IEI (F) of mEPSC. Data are expressed as means ± standard error of the mean. Statistical results were obtained using a two-way analysis of variance with the Aligned Rank Transform. *, $P < 0.05$, **, $P < 0.01$; simple main effect of 3wFS or ketamine. The number of animals and cells in each group for data acquisition were as follows: for sEPSCs: (animals, cells): noFS-VEH (3, 14), noFS-Ket (4, 9), 3wFS-VEH (4, 22), and 3wFS-Ket (3, 19); for mEPSCs: noFS-VEH (3, 15), noFS-Ket (4, 15), 3wFS-VEH (3, 12), and 3wFS-Ket (3, 15). noFS-VEH: non-footshock + vehicle administration; noFS-Ket: non-footshock + ketamine treatment; 3wFS-VEH: 3-week footshock + vehicle administration; 3wFS-Ket: 3-week footshock + ketamine treatment; spontaneous excitatory postsynaptic currents; mEPSC; miniature excitatory postsynaptic currents; PL: prelimbic; IEI: inter-event interval

Fig. 5. Ketamine induces distinct alterations in the inhibitory postsynaptic currents

(A) Representative recordings of sIPSCs in each group. (B and C) Amplitude (B) and IEI (C) of sIPSCs. (D) Representative recordings of mIPSCs in each group. (E and F) Amplitude (E) and IEI (F) of mIPSCs. Bars represent the means ± standard error of the mean. Statistical results were obtained using a two-way analysis of variance with the Aligned Rank Transform. ##, $P < 0.01$; main effect of ketamine. *, $P < 0.05$; main effect of 3wFS. The numbers of animals and cells in each group used for data acquisition were as follows: for sIPSCs (animals, cells): noFS-VEH (2, 12), noFS-Ket (3, 7), 3wFS-VEH (2, 12), and 3wFS-Ket (3, 13). For mIPSCs (animals, cells): noFS-VEH (3, 10), noFS-Ket (3, 6), 3wFS-VEH (2, 9), and 3wFS-Ket (3, 12). noFS-VEH: non-footshock + vehicle administration; noFS-Ket: non-footshock + ketamine treatment; 3wFS-VEH: 3-week footshock + vehicle administration; 3wFS-Ket: 3-week footshock + ketamine treatment; IPSCs: inhibitory postsynaptic currents; spontaneous inhibitory postsynaptic currents; mIPSCs: miniature inhibitory postsynaptic currents; IEI: inter-event interval

Fig. 6. Ketamine reversed the E/I ratio of the inter-event interval

(A) E/I ratio of charge. (B) E/I ratio of IEI. sEPSCs and sIPSCs were obtained from the same cells, and the E/I ratios were calculated by dividing the charge or IEI of sEPSCs by those of IPSCs. Bars represent the means ± standard error of the mean. Statistical results

were obtained using a two-way analysis of variance. *, $P < 0.05$, **, $P < 0.01$; simple main effect of 3wFS or ketamine. The numbers of animals and cells in each group used for data acquisition were as follows (animals, cells): noFS-VEH (2, 8), noFS-Ket (3, 6), 3wFS-VEH (2, 11), and 3wFS-Ket (3, 11). noFS-VEH: non-footshock + vehicle administration; noFS-Ket: non-footshock + ketamine treatment; 3wFS-VEH: 3-week footshock + vehicle administration; 3wFS-Ket: 3-week footshock + ketamine treatment; sIPSCs: spontaneous inhibitory postsynaptic currents; sEPSCs: spontaneous excitatory postsynaptic currents; IEI: inter-event interval; E/I: excitatory/inhibitory

Fig. 7. Ketamine did not rescue spine density, but increased the proportion of the mature spines

(A) A typical image of a PL layer V pyramidal cell showing the area from which the spine data were obtained. (B and C) Spine density (B) and the proportion of mature spines (C) in the apical dendrite. (D) Representative fluorescent images of apical dendritic spines in each group. (E and F) Spine density (E) and the proportion of matured spines (F) in the basal dendrite. (G) Representative images of basal dendritic spines in each group. Scale bar, 5 μm. Data are shown as mean ± standard error of the mean. Statistics were calculated by two-way analysis of variance. **, $P < 0.01$; main effect of 3wFS. ##, $P < 0.01$; main

effect of ketamine. The number of animals and cells in each group were as follows: for apical dendritic spines (animals, cells): noFS-VEH (3, 11), noFS-Ket (3, 10), 3wFS-VEH (4, 12), and 3wFS-Ket (4, 10); for basal dendritic spines (animals, cells): noFS-VEH (7, 11), noFS-Ket (3, 10), 3wFS-VEH (6, 11), and 3wFS-Ket (4, 13). PL: prelimbic; noFS-VEH: non-footshock + vehicle administration; noFS-Ket: non-footshock + ketamine treatment; 3wFS-VEH: 3-week footshock + vehicle administration; 3wFS-Ket: 3-week footshock + ketamine treatment.

Supplementary Figure Legends

Fig. S1. Dose-dependent effects of ketamine on the immobility counts

Ketamine 1 mg/kg did not reverse immobility counts. Data are shown as mean ± standard error of the mean. Statistical analysis was not performed as the data of ketamine 0 mg/kg and 10 mg/kg were the same as those of 3wFS-VEH and 3wFS-Ket in Fig. 2, respectively. There were 7 animals in each group. 3wFS-VEH: 3-week footshock + vehicle administration; 3wFS-Ket: 3-week footshock + ketamine treatment

Fig. S2. 3wFS did not induce a difference in the sucrose preference test.

Baseline sucrose preference of animals subjected to no foot shock versus three-week foot shock exposure. No significant difference in sucrose preference was noted between the groups. (Student's t-test: $t(12) = 0.893$, $P = 0.39$). Data expressed as the means ± standard error of the mean. Seven rats were used in each group.

Fig. S3. Ketamine did not alter the membrane characteristics in the infralimbic layer V pyramidal cells.

(A and B) Membrane potential changes evoked by positive current injection (A) and representative recordings (B) in IL layer V pyramidal cells. (C and D) Membrane

resistance (C) and RMP (D). Statistics were calculated by a three-way or two-way analysis of variance. No significant difference was detected in IL layer V pyramidal cells. The numbers of animals and cells in each group used for data acquisition were as follows (animals, cells): noFS-VEH (5, 9), noFS-Ket (3, 9), 3wFS-VEH (3, 8), and 3wFS-Ket (5, 9). Data are expressed as mean ± standard error of the mean. IL: infralimbic; RMP: resting membrane potential; noFS-VEH: non-footshock + vehicle administration; noFS-Ket: noFS + ketamine treatment; 3wFS-VEH: 3-week footshock + vehicle administration; 3wFS-Ket: 3-week footshock + ketamine treatment.

References

Ago, Y., Tanabe, W., Higuchi, M., Tsukada, S., Tanaka, T., Yamaguchi, T., Igarashi, H., Yokoyama, R., Seiriki, K., Kasai, A., Nakazawa, T., Nakagawa, S., Hashimoto, K., Hashimoto, H., 2019. (R)-Ketamine Induces a Greater Increase in Prefrontal 5-HT Release Than (S)-Ketamine and Ketamine Metabolites via an AMPA Receptor-Independent Mechanism. Int J Neuropsychopharmacol. 22, 665-674.

Anda, R.F., Butchart, A., Felitti, V.J., Brown, D.W., 2010. Building a framework for global surveillance of the public health implications of adverse childhood experiences. Am J Prev Med. 39, 93-8.

Arborelius, L., Eklund, M.B., 2007. Both long and brief maternal separation produces persistent changes in tissue levels of brain monoamines in middle-aged female rats. Neuroscience. 145, 738-50.

Autry, A.E., Adachi, M., Nosyreva, E., Na, E.S., Los, M.F., Cheng, P.F., Kavalali, E.T., Monteggia, L.M., 2011. NMDA receptor blockade at rest triggers rapid behavioural antidepressant responses. Nature. 475, 91-5.

Bambico, F.R., Li, Z., Creed, M., De Gregorio, D., Diwan, M., Li, J., McNeill, S., Gobbi, G., Raymond, R., Nobrega, J.N., 2020. A Key Role for Prefrontocortical Small Conductance Calcium-Activated Potassium Channels in Stress Adaptation and Rapid Antidepressant Response. Cereb Cortex. 30, 1559-1572.

Berman, R.M., Cappiello, A., Anand, A., Oren, D.A., Heninger, G.R., Charney, D.S., Krystal, J.H., 2000. Antidepressant effects of ketamine in depressed patients. Biol Psychiatry. 47, 351-4.

Carreno, F.R., Donegan, J.J., Boley, A.M., Shah, A., DeGuzman, M., Frazer, A., Lodge, D.J., 2016. Activation of a ventral hippocampus-medial prefrontal cortex pathway is both necessary and sufficient for an antidepressant response to ketamine. Mol Psychiatry. 21, 1298-308.

Chen, J., Dong, B., Feng, X., Jiang, D., Chen, G., Long, C., Yang, L., 2020. Aberrant mPFC GABAergic synaptic transmission and fear behavior in neuroligin-2 R215H knock-in mice. Brain Res. 1730, 146671.

Chen, X., Shu, S., Bayliss, D.A., 2009. HCN1 channel subunits are a molecular substrate for hypnotic actions of ketamine. J Neurosci. 29, 600-9.

Cook, S.C., Wellman, C.L., 2004. Chronic stress alters dendritic morphology in rat medial prefrontal cortex. J Neurobiol. 60, 236-48.

Drevets, W.C., Price, J.L., Simpson, J.R., Todd, R.D., Reich, T., Vannier, M., Raichle, M.E., 1997. Subgenual prefrontal cortex abnormalities in mood disorders. Nature. 386, 824-

7.
Duman, R.S., Aghajanian, G.K., 2012. Synaptic dysfunction in depression: potential therapeutic targets. Science. 338, 68-72.
Duman, R.S., Aghajanian, G.K., Sanacora, G., Krystal, J.H., 2016. Synaptic plasticity and depression: new insights from stress and rapid-acting antidepressants. Nat Med. 22, 238-49.
Duman, R.S., 2018. Ketamine and rapid-acting antidepressants: a new era in the battle against depression and suicide. F1000Res. 7.
Ferguson, B.R., Gao, W.J., 2018. PV Interneurons: Critical Regulators of E/I Balance for Prefrontal Cortex-Dependent Behavior and Psychiatric Disorders. Front Neural Circuits. 12, 37.
Gatto, C.L., Broadie, K., 2010. Genetic controls balancing excitatory and inhibitory synaptogenesis in neurodevelopmental disorder models. Front Synaptic Neurosci. 2, 4.
Gerhard, D.M., Pothula, S., Liu, R.J., Wu, M., Li, X.Y., Girgenti, M.J., Taylor, S.R., Duman, C.H., Delpire, E., Picciotto, M., Wohleb, E.S., Duman, R.S., 2019. GABA interneurons are the cellular trigger for ketamine's rapid antidepressant actions. J Clin Invest.
Gould, T.D., Zarate, C.A., Jr., Thompson, S.M., 2019. Molecular Pharmacology and Neurobiology of Rapid-Acting Antidepressants. Annu Rev Pharmacol Toxicol. 59, 213-236.
Hamani, C., Diwan, M., Isabella, S., Lozano, A.M., Nobrega, J.N., 2010a. Effects of different stimulation parameters on the antidepressant-like response of medial prefrontal cortex deep brain stimulation in rats. J Psychiatr Res. 44, 683-7.
Hamani, C., Diwan, M., Macedo, C.E., Brandão, M.L., Shumake, J., Gonzalez-Lima, F., Raymond, R., Lozano, A.M., Fletcher, P.J., Nobrega, J.N., 2010b. Antidepressant-like effects of medial prefrontal cortex deep brain stimulation in rats. Biol Psychiatry. 67, 117-24.
Hamani, C., Temel, Y., 2012. Deep brain stimulation for psychiatric disease: contributions and validity of animal models. Sci Transl Med. 4, 142rv8.
Heim, C., Nemeroff, C.B., 2001. The role of childhood trauma in the neurobiology of mood and anxiety disorders: preclinical and clinical studies. Biol Psychiatry. 49, 1023-39.
Hetzler, B.E., Wautlet, B.S., 1985. Ketamine-induced locomotion in rats in an open-field. Pharmacol Biochem Behav. 22, 653-5.
Hiraide, S., Saito, Y., Matsumoto, M., Yanagawa, Y., Ishikawa, S., Kubo, Y., Inoue, S., Yoshioka, M., Togashi, H., 2012. Possible modulation of the amygdala on metaplasticity deficits in the hippocampal CA1 field in early postnatally stressed rats.

J Pharmacol Sci. 119, 64-72.
Ishikawa, T., Sahara, Y., Takahashi, T., 2002. A single packet of transmitter does not saturate postsynaptic glutamate receptors. Neuron. 34, 613-21.
Jutkiewicz, E.M., Torregrossa, M.M., Sobczyk-Kojiro, K., Mosberg, H.I., Folk, J.E., Rice, K.C., Watson, S.J., Woods, J.H., 2006. Behavioral and neurobiological effects of the enkephalinase inhibitor RB101 relative to its antidepressant effects. Eur J Pharmacol. 531, 151-9.
Kessler, R.C., Berglund, P., Demler, O., Jin, R., Koretz, D., Merikangas, K.R., Rush, A.J., Walters, E.E., Wang, P.S., Replication, N.C.S., 2003. The epidemiology of major depressive disorder: results from the National Comorbidity Survey Replication (NCS-R). JAMA. 289, 3095-105.
Kimura, S., Togashi, H., Matsumoto, M., Shiozawa, T., Ishida, J., Kano, S., Ohashi, A., Ishikawa, S., Yamaguchi, T., Yoshioka, M., Shimamura, K., 2011. Serotonin(1A) receptor-mediated synaptic response in the rat medial prefrontal cortex is altered by early life stress: in vivo and in vitro electrophysiological studies. Nihon Shinkei Seishin Yakurigaku Zasshi. 31, 9-15.
Kroon, T., van Hugte, E., van Linge, L., Mansvelder, H.D., Meredith, R.M., 2019. Early postnatal development of pyramidal neurons across layers of the mouse medial prefrontal cortex. Sci Rep. 9, 5037.
Krystal, J.H., Sanacora, G., Duman, R.S., 2013. Rapid-acting glutamatergic antidepressants: the path to ketamine and beyond. Biol Psychiatry. 73, 1133-41.
Ku, S.M., Han, M.H., 2017. HCN Channel Targets for Novel Antidepressant Treatment. Neurotherapeutics. 14, 698-715.
Li, N., Lee, B., Liu, R.J., Banasr, M., Dwyer, J.M., Iwata, M., Li, X.Y., Aghajanian, G., Duman, R.S., 2010. mTOR-dependent synapse formation underlies the rapid antidepressant effects of NMDA antagonists. Science. 329, 959-64.
Li, N., Liu, R.J., Dwyer, J.M., Banasr, M., Lee, B., Son, H., Li, X.Y., Aghajanian, G., Duman, R.S., 2011. Glutamate N-methyl-D-aspartate receptor antagonists rapidly reverse behavioral and synaptic deficits caused by chronic stress exposure. Biol Psychiatry. 69, 754-61.
Liu, R.J., Aghajanian, G.K., 2008. Stress blunts serotonin- and hypocretin-evoked EPSCs in prefrontal cortex: role of corticosterone-mediated apical dendritic atrophy. Proc Natl Acad Sci U S A. 105, 359-64.
Liu, R.J., Ota, K.T., Dutheil, S., Duman, R.S., Aghajanian, G.K., 2015. Ketamine Strengthens CRF-Activated Amygdala Inputs to Basal Dendrites in mPFC Layer V Pyramidal Cells in the Prelimbic but not Infralimbic Subregion, A Key Suppressor of Stress

Responses. Neuropsychopharmacology. 40, 2066-75.
Liu, X., Carter, A.G., 2018. Ventral Hippocampal Inputs Preferentially Drive Corticocortical Neurons in the Infralimbic Prefrontal Cortex. J Neurosci. 38, 7351-7363.
Lupien, S.J., McEwen, B.S., Gunnar, M.R., Heim, C., 2009. Effects of stress throughout the lifespan on the brain, behaviour and cognition. Nat Rev Neurosci. 10, 434-45.
Lyttle, K., Ohmura, Y., Konno, K., Yoshida, T., Izumi, T., Watanabe, M., Yoshioka, M., 2015. Repeated fluvoxamine treatment recovers juvenile stress-induced morphological changes and depressive-like behavior in rats. Brain Res. 1616, 88-100.
Maeng, S., Zarate, C.A., Du, J., Schloesser, R.J., McCammon, J., Chen, G., Manji, H.K., 2008. Cellular mechanisms underlying the antidepressant effects of ketamine: role of alpha-amino-3-hydroxy-5-methylisoxazole-4-propionic acid receptors. Biol Psychiatry. 63, 349-52.
Matsuzaki, H., Izumi, T., Horinouchi, T., Boku, S., Inoue, T., Yamaguchi, T., Yoshida, T., Matsumoto, M., Togashi, H., Miwa, S., Koyama, T., Yoshioka, M., 2011. Juvenile stress attenuates the dorsal hippocampal postsynaptic 5-HT1A receptor function in adult rats. Psychopharmacology (Berl). 214, 329-37.
Menke, A., Binder, E.B., 2014. Epigenetic alterations in depression and antidepressant treatment. Dialogues Clin Neurosci. 16, 395-404.
Miller, O.H., Moran, J.T., Hall, B.J., 2016. Two cellular hypotheses explaining the initiation of ketamine's antidepressant actions: Direct inhibition and disinhibition. Neuropharmacology. 100, 17-26.
Moda-Sava, R.N., Murdock, M.H., Parekh, P.K., Fetcho, R.N., Huang, B.S., Huynh, T.N., Witztum, J., Shaver, D.C., Rosenthal, D.L., Alway, E.J., Lopez, K., Meng, Y., Nellissen, L., Grosenick, L., Milner, T.A., Deisseroth, K., Bito, H., Kasai, H., Liston, C., 2019. Sustained rescue of prefrontal circuit dysfunction by antidepressant-induced spine formation. Science. 364.
Moench, K.M., Wellman, C.L., 2015. Stress-induced alterations in prefrontal dendritic spines: Implications for post-traumatic stress disorder. Neurosci Lett. 601, 41-5.
Mukai, H., Hatanaka, Y., Mitsuhashi, K., Hojo, Y., Komatsuzaki, Y., Sato, R., Murakami, G., Kimoto, T., Kawato, S., 2011. Automated analysis of spines from confocal laser microscopy images: application to the discrimination of androgen and estrogen effects on spinogenesis. Cereb Cortex. 21, 2704-11.
Oertner, T.G., Sabatini, B.L., Nimchinsky, E.A., Svoboda, K., 2002. Facilitation at single synapses probed with optical quantal analysis. Nat Neurosci. 5, 657-64.
Pešić, V., Petrović, J., M Jukić, M., 2016. Molecular Mechanism and Clinical Relevance of Ketamine as Rapid-Acting Antidepressant. Drug Dev Res. 77, 414-422.

Podkowa, K., Pochwat, B., Brański, P., Pilc, A., Pałucha-Poniewiera, A., 2016. Group II mGlu receptor antagonist LY341495 enhances the antidepressant-like effects of ketamine in the forced swim test in rats. Psychopharmacology (Berl). 233, 2901-14.

Radley, J.J., Sisti, H.M., Hao, J., Rocher, A.B., McCall, T., Hof, P.R., McEwen, B.S., Morrison, J.H., 2004. Chronic behavioral stress induces apical dendritic reorganization in pyramidal neurons of the medial prefrontal cortex. Neuroscience. 125, 1-6.

Sarkar, A., Kabbaj, M., 2016. Sex Differences in Effects of Ketamine on Behavior, Spine Density, and Synaptic Proteins in Socially Isolated Rats. Biol Psychiatry. 80, 448-456.

Scheinost, D., Holmes, S.E., DellaGioia, N., Schleifer, C., Matuskey, D., Abdallah, C.G., Hampson, M., Krystal, J.H., Anticevic, A., Esterlis, I., 2018. Multimodal Investigation of Network Level Effects Using Intrinsic Functional Connectivity, Anatomical Covariance, and Structure-to-Function Correlations in Unmedicated Major Depressive Disorder. Neuropsychopharmacology. 43, 1119-1127.

Schneider, C.A., Rasband, W.S., Eliceiri, K.W., 2012. NIH Image to ImageJ: 25 years of image analysis. Nat Methods. 9, 671-5.

Shikanai, H., Yoshida, T., Konno, K., Yamasaki, M., Izumi, T., Ohmura, Y., Watanabe, M., Yoshioka, M., 2012. Distinct neurochemical and functional properties of GAD67-containing 5-HT neurons in the rat dorsal raphe nucleus. J Neurosci. 32, 14415-26.

Sullivan, R.M., Gratton, A., 2002. Prefrontal cortical regulation of hypothalamic-pituitary-adrenal function in the rat and implications for psychopathology: side matters. Psychoneuroendocrinology. 27, 99-114.

Surges, R., Freiman, T.M., Feuerstein, T.J., 2004. Input resistance is voltage dependent due to activation of Ih channels in rat CA1 pyramidal cells. J Neurosci Res. 76, 475-80.

Treadway, M.T., Waskom, M.L., Dillon, D.G., Holmes, A.J., Park, M.T.M., Chakravarty, M.M., Dutra, S.J., Polli, F.E., Iosifescu, D.V., Fava, M., Gabrieli, J.D.E., Pizzagalli, D.A., 2015. Illness progression, recent stress, and morphometry of hippocampal subfields and medial prefrontal cortex in major depression. Biol Psychiatry. 77, 285-294.

Tsutsui-Kimura, I., Yoshida, T., Ohmura, Y., Izumi, T., Yoshioka, M., 2014. Milnacipran remediates impulsive deficits in rats with lesions of the ventromedial prefrontal cortex. Int J Neuropsychopharmacol. 18.

Tunnard, C., Rane, L.J., Wooderson, S.C., Markopoulou, K., Poon, L., Fekadu, A., Juruena, M., Cleare, A.J., 2014. The impact of childhood adversity on suicidality and clinical course in treatment-resistant depression. J Affect Disord. 152-154, 122-30.

Uylings, H.B., Groenewegen, H.J., Kolb, B., 2003. Do rats have a prefrontal cortex? Behav Brain Res. 146, 3-17.

Wang, M., Ramos, B.P., Paspalas, C.D., Shu, Y., Simen, A., Duque, A., Vijayraghavan, S.,

Brennan, A., Dudley, A., Nou, E., Mazer, J.A., McCormick, D.A., Arnsten, A.F., 2007. Alpha2A-adrenoceptors strengthen working memory networks by inhibiting cAMP-HCN channel signaling in prefrontal cortex. Cell. 129, 397-410.

WHO, 2018. Depression [http://www.who.int/en/news-room/fact-sheets/detail/depression (2018.10.28)].

Wilkinson, S.T., Ballard, E.D., Bloch, M.H., Mathew, S.J., Murrough, J.W., Feder, A., Sos, P., Wang, G., Zarate, C.A., Sanacora, G., 2018. The Effect of a Single Dose of Intravenous Ketamine on Suicidal Ideation: A Systematic Review and Individual Participant Data Meta-Analysis. Am J Psychiatry. 175, 150-158.

Willner, P., Towell, A., Sampson, D., Sophokleous, S., Muscat, R., 1987. Reduction of sucrose preference by chronic unpredictable mild stress, and its restoration by a tricyclic antidepressant. Psychopharmacology (Berl). 93, 358-64.

Wobbrock, J., Findlater, L., Gergle, D., Higgins, J., 2011. The Aligned Rank Transform for Nonparametric Factorial Analyses Using Only ANOVA Procedures. Vol. 2011.

Workman, E.R., Niere, F., Raab-Graham, K.F., 2018. Engaging homeostatic plasticity to treat depression. Mol Psychiatry. 23, 26-35.

Wu, C., Wang, Y., He, Y., Wu, S., Xie, Z., Zhang, J., Shen, J., Wang, Z., He, L., 2020. Sub-anesthetic and anesthetic ketamine produce different long-lasting behavioral phenotypes (24 h post-treatment) via inducing different brain-derived neurotrophic factor (BDNF) expression level in the hippocampus. Neurobiol Learn Mem. 167, 107136.

Xue, M., Atallah, B.V., Scanziani, M., 2014. Equalizing excitation-inhibition ratios across visual cortical neurons. Nature. 511, 596-600.

Yamamuro, K., Yoshino, H., Ogawa, Y., Makinodan, M., Toritsuka, M., Yamashita, M., Corfas, G., Kishimoto, T., 2018. Social Isolation During the Critical Period Reduces Synaptic and Intrinsic Excitability of a Subtype of Pyramidal Cell in Mouse Prefrontal Cortex. Cereb Cortex. 28, 998-1010.

Yu, H., Li, M., Zhou, D., Lv, D., Liao, Q., Lou, Z., Shen, M., Wang, Z., Li, M., Xiao, X., Zhang, Y., Wang, C., 2018. Vesicular glutamate transporter 1 (VGLUT1)-mediated glutamate release and membrane GluA1 activation is involved in the rapid antidepressant-like effects of scopolamine in mice. Neuropharmacology. 131, 209-222.

Zanos, P., Moaddel, R., Morris, P.J., Georgiou, P., Fischell, J., Elmer, G.I., Alkondon, M., Yuan, P., Pribut, H.J., Singh, N.S., Dossou, K.S., Fang, Y., Huang, X.P., Mayo, C.L., Wainer, I.W., Albuquerque, E.X., Thompson, S.M., Thomas, C.J., Zarate, C.A., Gould, T.D., 2016. NMDAR inhibition-independent antidepressant actions of ketamine metabolites. Nature. 533, 481-6.

Zanos, P., Thompson, S.M., Duman, R.S., Zarate, C.A., Gould, T.D., 2018. Convergent Mechanisms Underlying Rapid Antidepressant Action. CNS Drugs. 32, 197-227.

Zarate, C., Duman, R.S., Liu, G., Sartori, S., Quiroz, J., Murck, H., 2013. New paradigms for treatment-resistant depression. Ann N Y Acad Sci. 1292, 21-31.

Zarate, C.A., Singh, J.B., Carlson, P.J., Brutsche, N.E., Ameli, R., Luckenbaugh, D.A., Charney, D.S., Manji, H.K., 2006. A randomized trial of an N-methyl-D-aspartate antagonist in treatment-resistant major depression. Arch Gen Psychiatry. 63, 856-64.

Zhu, X., Ye, G., Wang, Z., Luo, J., Hao, X., 2017. Sub-anesthetic doses of ketamine exert antidepressant-like effects and upregulate the expression of glutamate transporters in the hippocampus of rats. Neurosci Lett. 639, 132-137.

A

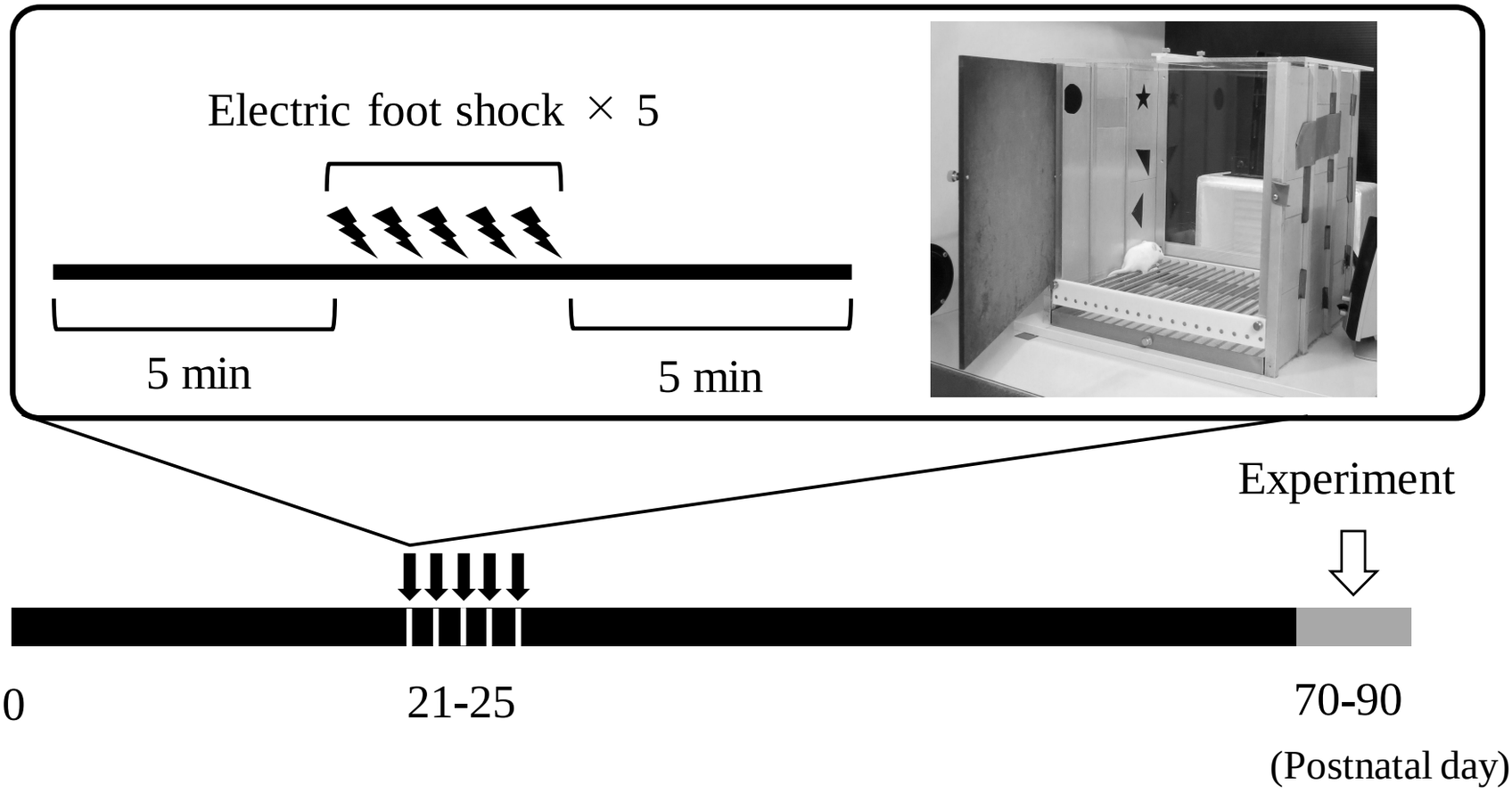
Electric foot shock × 5
5 min
5 min
Experiment
0
21-25
70-90
(Postnatal day)

B

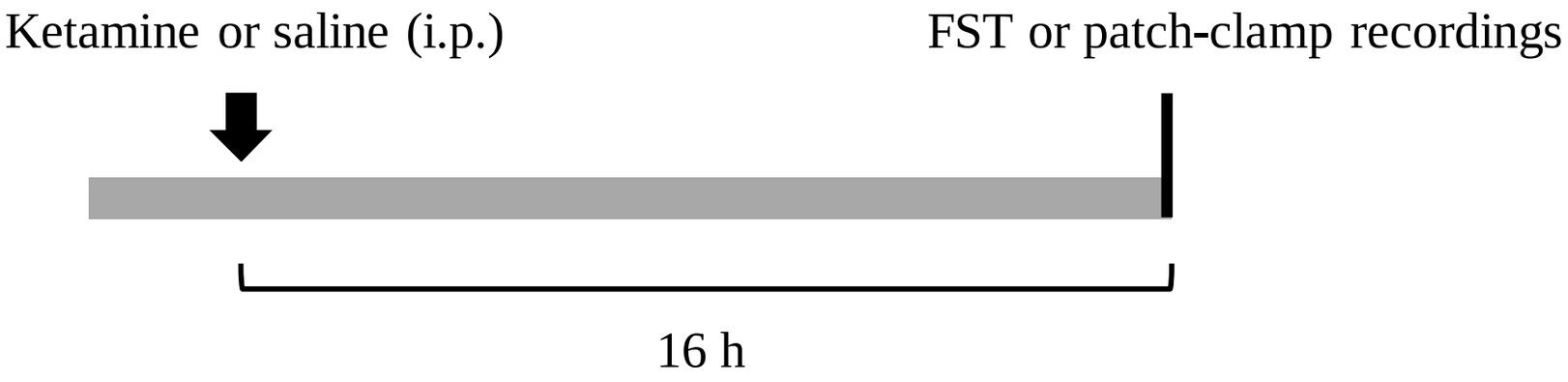
Ketamine or saline (i.p.)
FST or patch-clamp recordings
16 h

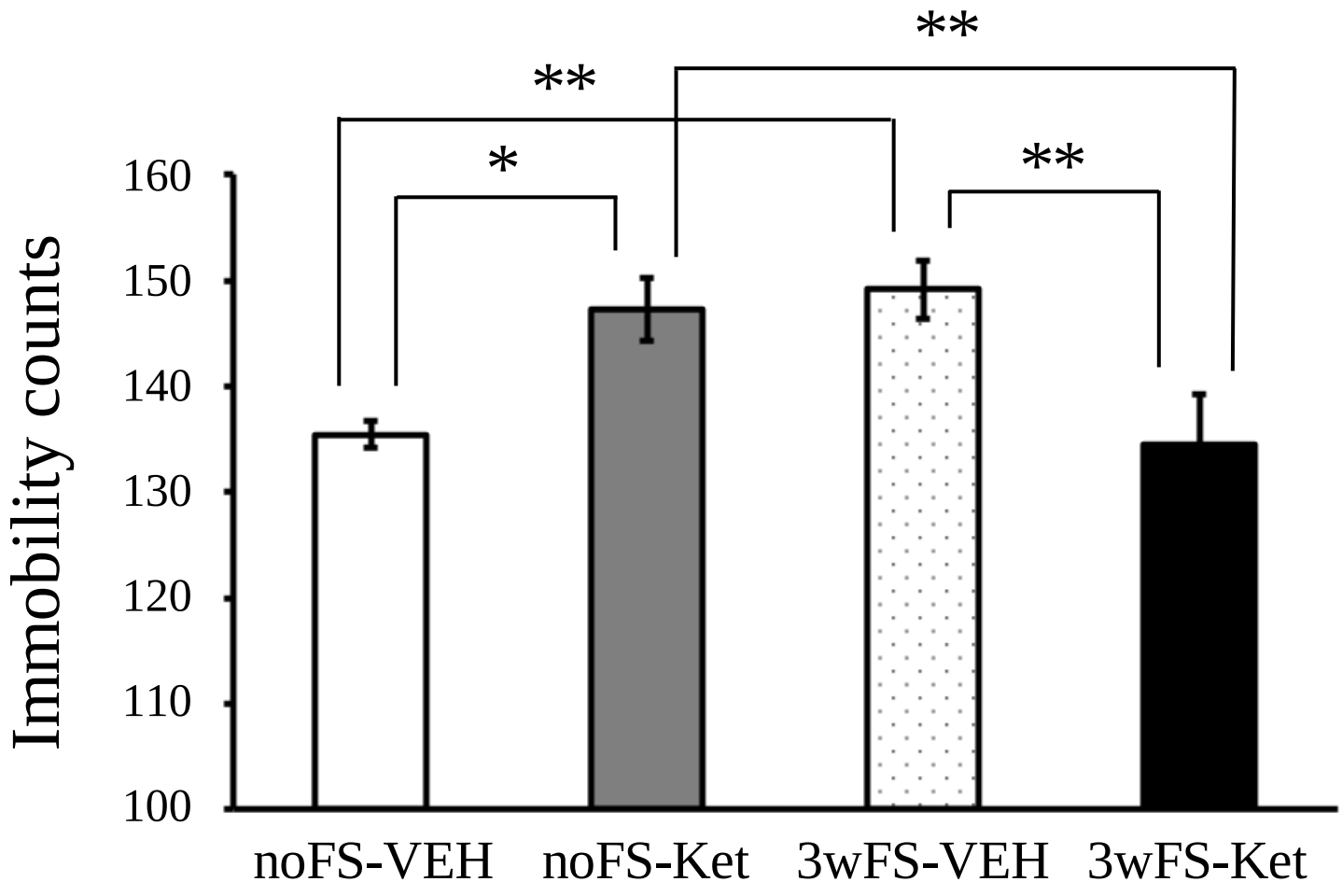
**
**
*
**
160
150
140
130
120
110
100
Immobility counts
noFS-VEH
noFS-Ket
3wFS-VEH
3wFS-Ket

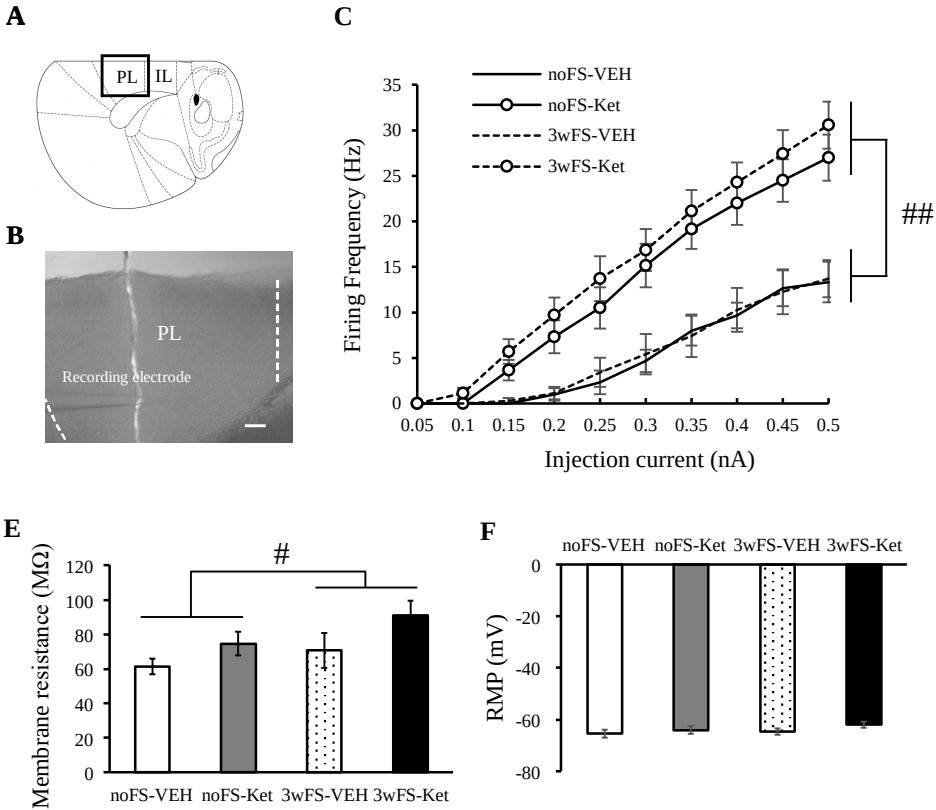
A
PL
IL
B
PL
Recording electrode
C
noFS-VEH
noFS-Ket
3wFS-VEH
3wFS-Ket
Firing Frequency (Hz)
Injection current (nA)
##
D
noFS-VEH
noFS-Ket
3wFS-VEH
3wFS-Ket
20 mV
0.5 nA
0.05 s
E
Membrane resistance (MΩ)
#
noFS-VEH
noFS-Ket
3wFS-VEH
3wFS-Ket
F
RMP (mV)
noFS-VEH
noFS-Ket
3wFS-VEH
3wFS-Ket

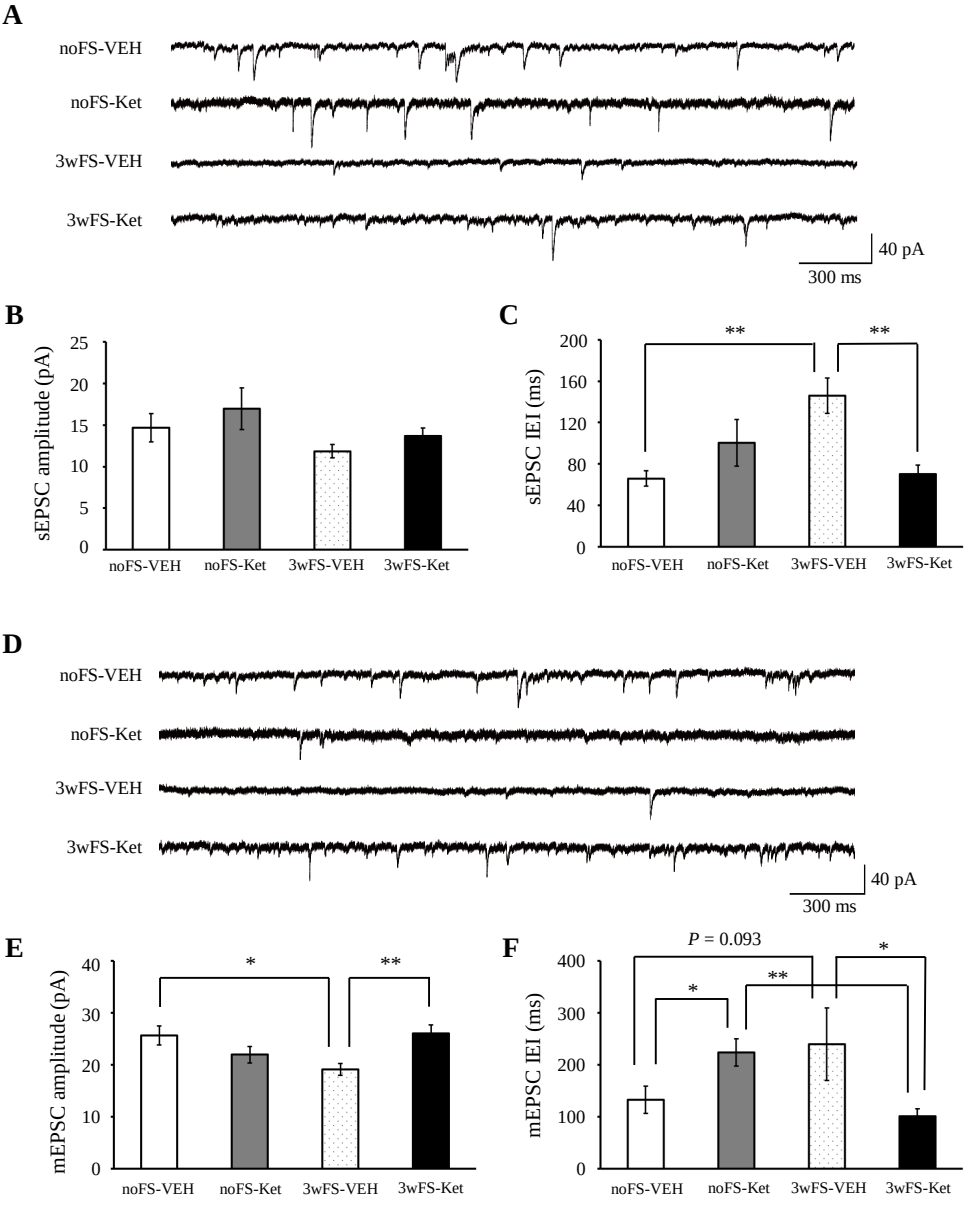
A
noFS-VEH
noFS-Ket
3wFS-VEH
3wFS-Ket
40 pA
300 ms
B
sEPSC amplitude (pA)
25
20
15
10
5
0
noFS-VEH
noFS-Ket
3wFS-VEH
3wFS-Ket
C
sEPSC IEI (ms)
200
160
120
80
40
0
**
**
noFS-VEH
noFS-Ket
3wFS-VEH
3wFS-Ket
D
noFS-VEH
noFS-Ket
3wFS-VEH
3wFS-Ket
40 pA
300 ms
E
mEPSC amplitude (pA)
40
30
20
10
0
*
**
noFS-VEH
noFS-Ket
3wFS-VEH
3wFS-Ket
F
P = 0.093
mEPSC IEI (ms)
400
300
200
100
0
*
**
*
noFS-VEH
noFS-Ket
3wFS-VEH
3wFS-Ket

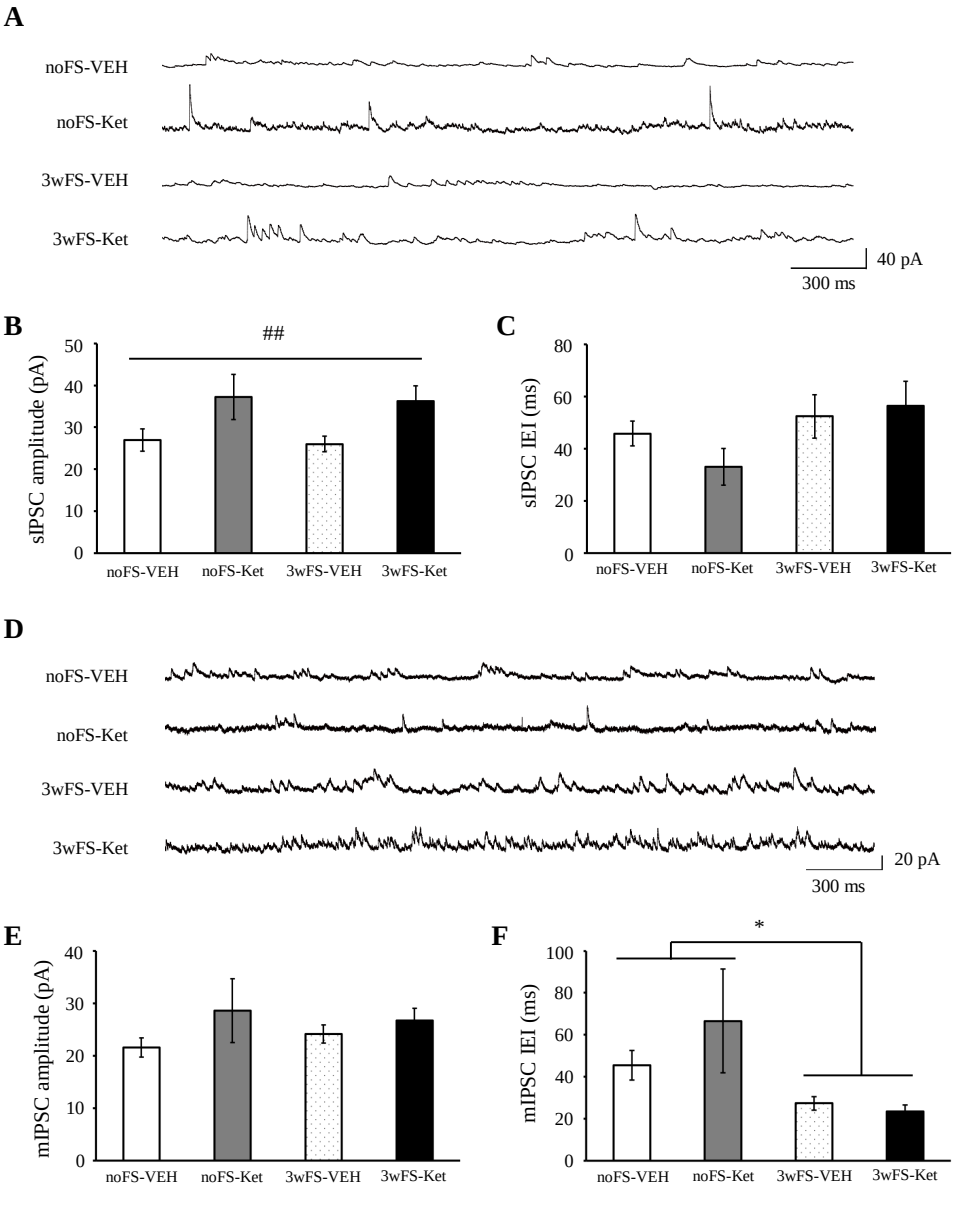
A
noFS-VEH
noFS-Ket
3wFS-VEH
3wFS-Ket
40 pA
300 ms
B
##
sIPSC amplitude (pA)
50
40
30
20
10
0
noFS-VEH
noFS-Ket
3wFS-VEH
3wFS-Ket
C
sIPSC IEI (ms)
80
60
40
20
0
noFS-VEH
noFS-Ket
3wFS-VEH
3wFS-Ket
D
noFS-VEH
noFS-Ket
3wFS-VEH
3wFS-Ket
20 pA
300 ms
E
mIPSC amplitude (pA)
40
30
20
10
0
noFS-VEH
noFS-Ket
3wFS-VEH
3wFS-Ket
F
*
mIPSC IEI (ms)
100
80
60
40
20
0
noFS-VEH
noFS-Ket
3wFS-VEH
3wFS-Ket

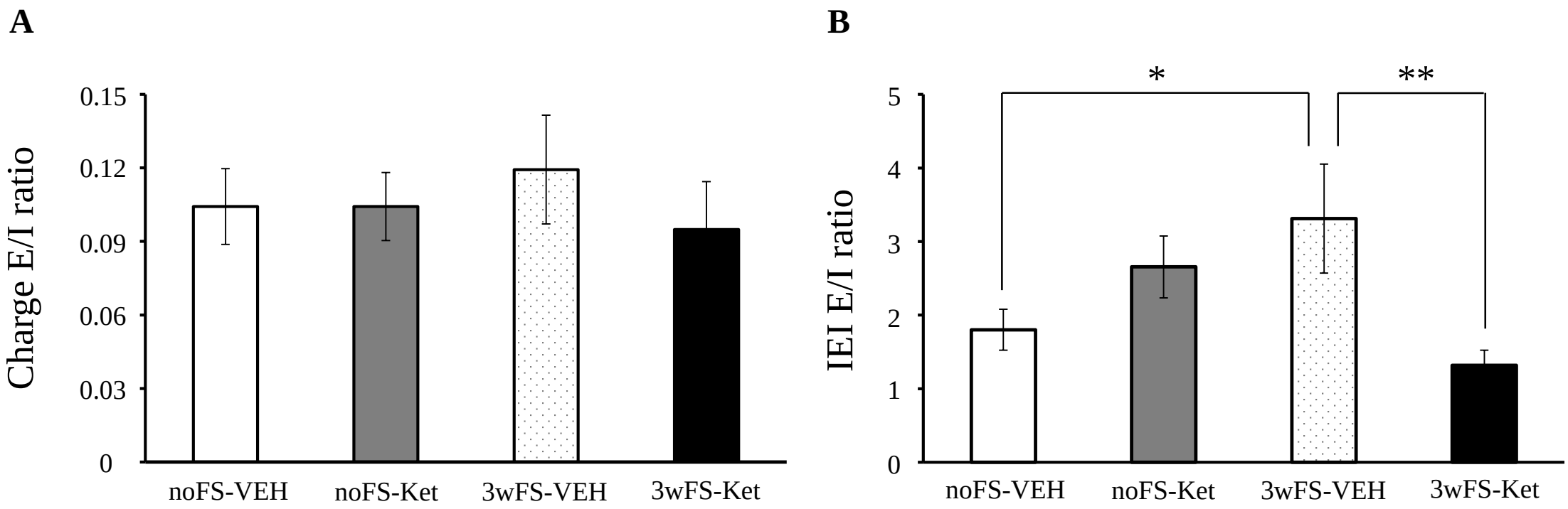
A
Charge E/I ratio
0.15
0.12
0.09
0.06
0.03
0
noFS-VEH
noFS-Ket
3wFS-VEH
3wFS-Ket
B
IEI E/I ratio
*
**
5
4
3
2
1
0
noFS-VEH
noFS-Ket
3wFS-VEH
3wFS-Ket

A

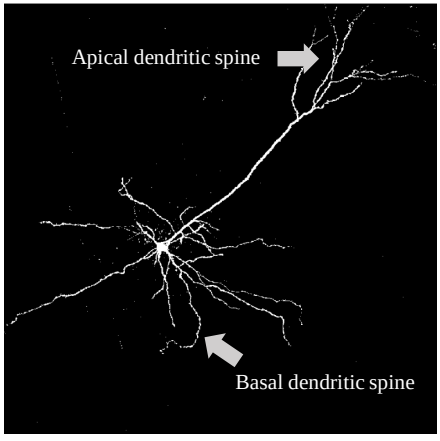
Apical dendritic spine
Basal dendritic spine

B

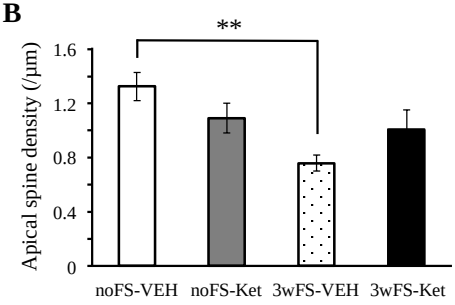
**
Apical spine density (/μm)
1.6
1.2
0.8
0.4
0
noFS-VEH
noFS-Ket
3wFS-VEH
3wFS-Ket

C

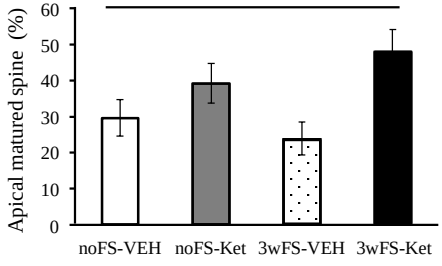
##
Apical matured spine (%)
60
50
40
30
20
10
0
noFS-VEH
noFS-Ket
3wFS-VEH
3wFS-Ket

D

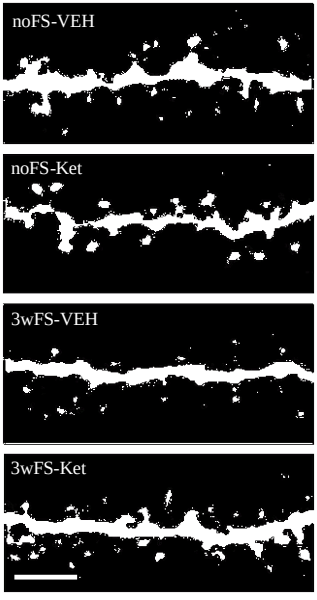
noFS-VEH
noFS-Ket
3wFS-VEH
3wFS-Ket

E

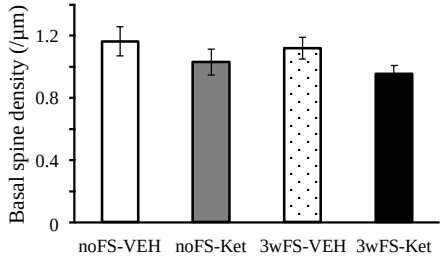
Basal spine density (/μm)
1.2
0.8
0.4
0
noFS-VEH
noFS-Ket
3wFS-VEH
3wFS-Ket

F

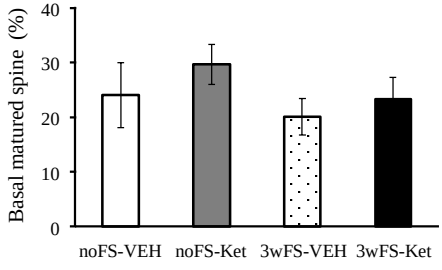
Basal matured spine (%)
40
30
20
10
0
noFS-VEH
noFS-Ket
3wFS-VEH
3wFS-Ket

G

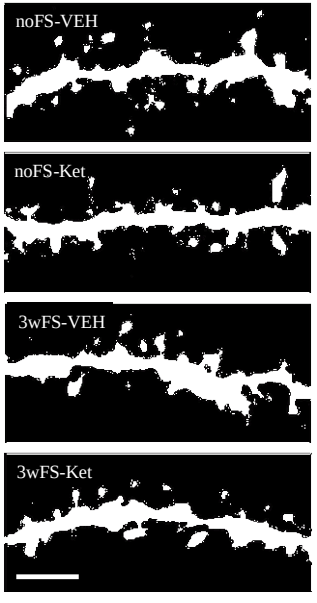
noFS-VEH
noFS-Ket
3wFS-VEH
3wFS-Ket